Bakare, M.S. and Voisey, K.T. and Roe, M.J. and McCartney, D.G. (2010) X-ray photoelectron spectroscopy study of the passive films formed on thermally sprayed and wrought Inconel 625. Applied Surface Science, 257 (3). pp. 786-794. ISSN 0169-4332

X-ray Photoelectron Spectroscopy Study of the Passive Films formed on Thermally Sprayed and Wrought Inconel 625.

M.S. Bakare, K.T. Voisey, M.J. Roe, D.G. McCartney

Materials, Mechanics and Structures Research Division,

Faculty of Engineering, University of Nottingham, Nottingham, NG7 2RD, UK.

Corresponding Author: Katy.voisey@nottingham.ac.uk Tel: +44 115 951 4139

Abstract

There is a well known performance gap in corrosion resistance between thermally sprayed corrosion resistant coatings and the equivalent bulk materials. Interconnected porosity has an important and well known effect, however there are additional relevant microstructural effects. Previous work has shown that a compositional difference exists between the regions of resolidified and non-melted material that exist in the as-sprayed coatings. The resolidified regions are depleted in oxide forming elements due to formation of oxides during coating deposition. Formation of galvanic cells between these different regions is believed to decrease the corrosion resistance of the coating. In order to increase understanding of the details of this effect, this work uses X-ray photoelectron spectroscopy (XPS) to study the passive films formed on thermally sprayed coatings (HVOF) and bulk Inconel 625, a commercially available corrosion resistant Ni-Cr-Mo-Nb alloy. Passive films produced by potentiodynamic scanning to 400mV in 0.5M sulphuric acid were compared with air formed films. The poorer corrosion performance of the thermally sprayed coatings was attributed to $Ni(OH)_2$, which forms a loose, non-adherent and therefore non-protective film. The good corrosion resistance of wrought Inconel 625 is due to formation of Cr, Mo and Nb oxides.

Keywords: Inconel 625 alloy, HVOF thermally sprayed coating, x-ray photoelectron spectroscopy, binding energy, passive films.

1 Introduction

Inconel 625 is a solid solution strengthened nickel-based corrosion resistant alloy which is widely used as a thermally sprayed coating for corrosion protection of components in thermal and nuclear energy environments as well as other aqueous corrosive environments [1]. Thermally sprayed corrosion resistant coatings are widely used to enhance corrosion resistance. Such coatings do usefully improve corrosion resistance, however, there is a well established performance gap between the coating and the equivalent bulk material [2-5]. This is attributed to the characteristic microstructure of the thermally sprayed coating. Thermally sprayed coatings are built up from the successive impacts of partially or fully melted particles. This results in a distinctive lamellar structure which includes some porosity and regions of resolidified material. Oxides may also be incorporated into the coating since, depending on the thermal spraying technique used, the hot particles can partially oxidise as they travel between the spray gun and the substrate.

The presence of interconnected porosity has an important and well known effect, it simply links the "coated" substrate to the corrosive environment, undermining the barrier function of the coating. There are also additional relevant microstructural effects due to other features. There is a compositional difference between regions of resolidified and non-melted material in as-sprayed coatings. The resolidified regions are depleted in oxide forming elements due to formation of oxides during coating deposition [4, 6]. Previous work by the present authors has shown that formation of galvanic cells between these different regions decreases the corrosion resistance of the coating, resulting in the observed performance gap [6]. The details of how these microgalvanic cells affect oxide formation are not yet fully understood and are the topic of this paper.

Previous XPS work on Inconel 625 has mainly focused on the analysis of oxides formed on wrought material in corrosive and oxidising environments such as supercritical water reactors [7]. Under such conditions a duplex scale with a thickness of the order of 1 micron is formed, with an outer layer including the Ni containing compounds NiO, $Ni(OH)_2$ and $NiCr_2O_4$ [7]. $Ni(OH)_2$ was also detected in the outer layer of the oxide film formed in a heated, 250-200ºC, lithium borate buffer solution [8]. The work presented in this paper considers air grown films, these are significantly thinner with typical thicknesses of a few nanometers [9]. Lloyd et al. [9] report the presence of NiO, Cr_2O_3 and MoO_3 in the air formed film on Inconel 625. Neville and Hodgkiess [10] report Fe^{2+} and Fe^{3+} oxides as well as signals from Cr oxide and Mo oxide in the air formed film, but state that no Ni oxides or hydroxides were detected. It is possible that Lloyd et al. [9] detected metallic Ni in the underlying alloy below the thin air formed oxide layer, this would be consistent with their SIMS observation of Ni enrichment at the alloy surface. No published work on compositional analysis of passive films on HVOF sprayed Inconel 625 has been found. The aim of this paper is to use XPS to analyse the passive films on wrought and high velocity oxy-fuel (HVOF) thermally sprayed Inconel 625. Both air formed films and the films formed due to potentiodynamic polarisation to the passive region are included.

2 Experimental Procedures

2.1 Materials and Sample Preparation

5mm thick wrought Inconel 625 plate, obtained from Special Metals Corporation, Hereford, UK, was used as the reference material for this work. The chemical composition is as shown in Table 1. A gas-atomised Inconel 625 powder, with nominal size range -53+20 μm, and the composition given in Table 1, was used as the feedstock material for the HVOF coatings.

2.2 Thermal spraying process

Inconel 625 HVOF coatings were deposited on 60x40x5 mm mild steel substrates using a metjet-II HVOF spray gun from Metallisation Limited, Dudley. The spraying conditions for the coating are stated in Table 2. Before coating deposition, the substrates were cleaned with detergent, degreased with industrial methylated spirit and grit blasted with brown alumina grit.

2.3 Corrosion tests

Potentiodynamic polarisation scans in 0.5M H_2SO_4 were carried out using an ACM Instruments potentiostat. The experiment was set up according to ASTM standard G5-94 with a three electrode cell: working electrode (WE), platinum auxiliary electrode (AE) and calomel reference electrode (RE). For both wrought alloy and coated samples, the surfaces were polished to 1µm with approximately 1cm^2 area exposed to electrolyte. Nitrogen gas was used to purge the solution to remove oxygen dissolved in it. Stabilisation at open circuit potential was carried out for 1h before polarisation. The potentiodynamic scan was performed at a temperature of 30^oC with a 20mV/min sweep rate. Full polarisation curves, up to a maximum potential of 1000mV, were obtained to demonstrate the performance gap between wrought and HVOF sprayed Inconel 625. For XPS analysis, additional samples underwent partial potentiodynamic scans, with the experiments were stopping within the passivating

region at a potential of 400mV for all samples, as shown in

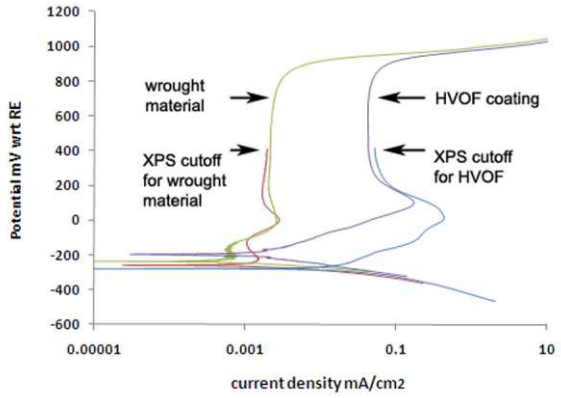

Figure 1.

2.4 Sample characterisation

Each of the samples was observed after etching in aqua regia solution for about 10 seconds: solution containing 3 volumes of 37% HCl and 1 volume of 69% HNO_3, heated to 30-40^{o}C. Samples were characterised using SEM and optical microscopy.

Oxygen content analysis was carried out by London and Scandinavian Metallurgical Co. Ltd, Rotherham, UK with their TC-436AR analyser.

Porosity of the coatings was determined by image analysis of cross-sectional images using ImageJ software. The standard errors shown were obtained from 5 repeats of measurements.

2.5 X-ray photoelectron spectroscopy measurement

Samples were washed with de-ionised water and industrial methylated spirit and dried before being transferred into the ultra-high vacuum XPS chamber environment. Argon ion cleaning was not performed. General survey spectra and high resolution spectra of the principal element photoelectron peaks were collected for wrought material and HVOF coatings both

before and after potentiodynamic polarisation to 400mV. The time between the end of corrosion testing and samples being placed into the XPS was approximately 10 minutes.

The instrument used was a VG Scientific ESCALab Mark I photoelectron spectrometer utilising non-monochromatic AlKα with excitation energy of 1486.6eV and a vacuum pressure of approximately 1 x 10^{-9} mbar. Charge correction was made with respect to the C1s peak at 285 eV.

The survey spectra of the specimens cover the full range of binding energies (0 to 1100 eV). High resolution spectra for Ni and Cr were obtained from the most intense photoelectron line: the Ni2p and Cr2p doublets, with individual scans covering the full range of the $2p_{3/2}$ and $2p_{1/2}$ doublets separation, 848-880eV and 570-592eV for Ni and Cr respectively. High resolution scans for Mo and Nb were carried out at 225-240eV and 202-213eV respectively in order to cover the 3d doublets, the most intense photoelectron lines for these elements.

Data reduction and peak fitting of the Ni2p, Cr2p, Mo3d and Nb3d regions were made using the CasaXPS software package, with peak deconvolution carried out using a Gaussian-Lorentzian (30:70) peak shape and a non-linear (Shirley) background model. The binding energies and peak shapes were used to identify the species present. The area ratios allow, for a given element, the relative proportions of atoms in each different binding state to be determined (see appendices).

3 Results

3.1 Microstructure

The microstructure of wrought Inconel 625 is shown in

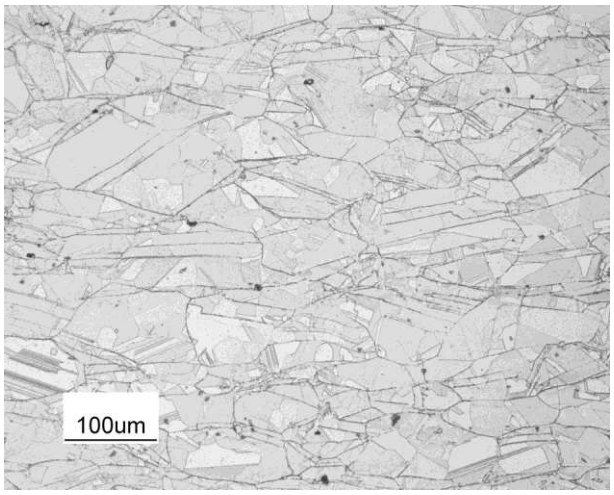

Figure **2**. Previous analysis of the same material by Ahmed et al. [6], show it to be a γ-Ni based alloy with a face centred cubic structure containing a small amount of second phase particles present. These particles contain Ti and Nb and attributed as carbides, nitrides or carbonitrides [6]. The presence of sub-grains and twins is indicative of prior cold rolling and annealing [6].

The as-sprayed coating had a thickness of 350-400µm (Figure 3a). The coating is built up from the successive impacts of individual powder particles that are heated and accelerated towards the substrate by the spraying process. On arrival at the substrate the particles are fully or partially molten. On impact molten material spreads out and resolidifies whereas non-molten material deforms and adheres mainly by mechanical interlocking. The coating microstructure shown in Figure 3b is typical of HVOF metallic coatings and has been discussed in detail in previous work [4]. Individual particles, or splats, can be seen, it is also clear that the coating consists of two distinct types of material: deformed non-melted material and areas of resolidified material. Previous work [6] has identified a difference in the composition of these two types of material, with the resolidified material being depleted in Cr due to oxidation during the spraying process. As is typical of all thermally sprayed coatings,

the coating also has some oxide and porosity content. These were determined to be 2.2 ± 0.02 wt % and 1.2 ± 0.1 vol % respectively (Table 3), values typical of HVOF sprayed metallic coatings. Oxide content was determined from the oxygen content results from London and Scandinavian Metallurgical Co. Ltd, assuming that all oxygen present was in the form of Cr_2O_3. This assumption is based on previous work that has identified the oxide formed during spraying as Cr_2O_3 [4, 6].

3.2 Potentiodynamic polarisation results

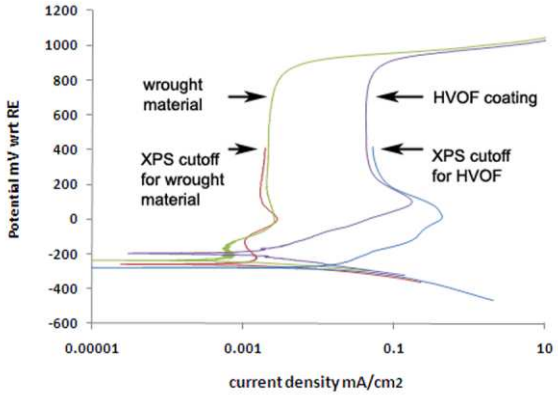

The potentiodynamic results shown in Figure **1** confirm the performance gap between the HVOF sprayed Inconel 625 coating and the wrought material. The E_{corr} values for all samples are similar, falling in the range of -190 to -280 mV. The greater variation seen for the coated samples is attributed to the sample to sample variation in microstructure that is expected of thermally sprayed coatings. Both versions of the material show a passive region, however the corrosion current density in this region is significantly greater for the coating than for the wrought material. Observed current densities are 0.002 mA cm^{-2} and 0.050 mA cm^{-2} for the wrought material and sprayed coating respectively.

3.3 XPS results

Figure 4 and Figure 5 show the XPS survey spectra with peaks of nickel, chromium, molybdenum, niobium, carbon and oxygen clearly visible. Both Auger and photoelectron peaks are labelled, however only photoelectron peaks are used in the following analysis.

The experimental binding energy values of O1s, C1s, Ni2p, Cr2p, Mo3d and Nb3d all matched well with the reference database values. Using the reference binding energies for possible oxide structures, peaks corresponding to NiO, Cr_2O_3, MoO_2, MoO_3, NbO and Nb_2O_5 were identified in both the wrought and coated samples, details of the species identified are presented in Appendix A and Appendix B. Charge correction was performed with respect to the C1s peak at 285eV, which was common to all samples and was attributed to adventitious carbon contamination [11]. The satellite peak of the Ni2p region both for the metal and oxide form is a well known feature associated with some elements such as Ni [12], however our analysis only considers the main photoelectric peaks. Detailed interpretation of the Mo peak was complicated due to overlapping of the oxide peaks [13], hence we restricted our comments on Mo to the relative contributions of the metallic and total Mo oxide contributions.

3.3.1 Samples before polarisation corrosion test

Metallic peaks of Ni2p, Cr2p and Mo3d as well as their corresponding oxides were seen in both samples. No metallic peak of Nb3d was detected in either the coating or the wrought alloy.

The O1s peak at 530.42eV indicated the presence of oxides. For both wrought alloy and coating, the ratio of areas under the Ni2p peak indicated that the majority of the Ni at the surface was metallic, rather than oxidised. NiO was the only oxide of nickel assigned.

The Cr2p spectra in

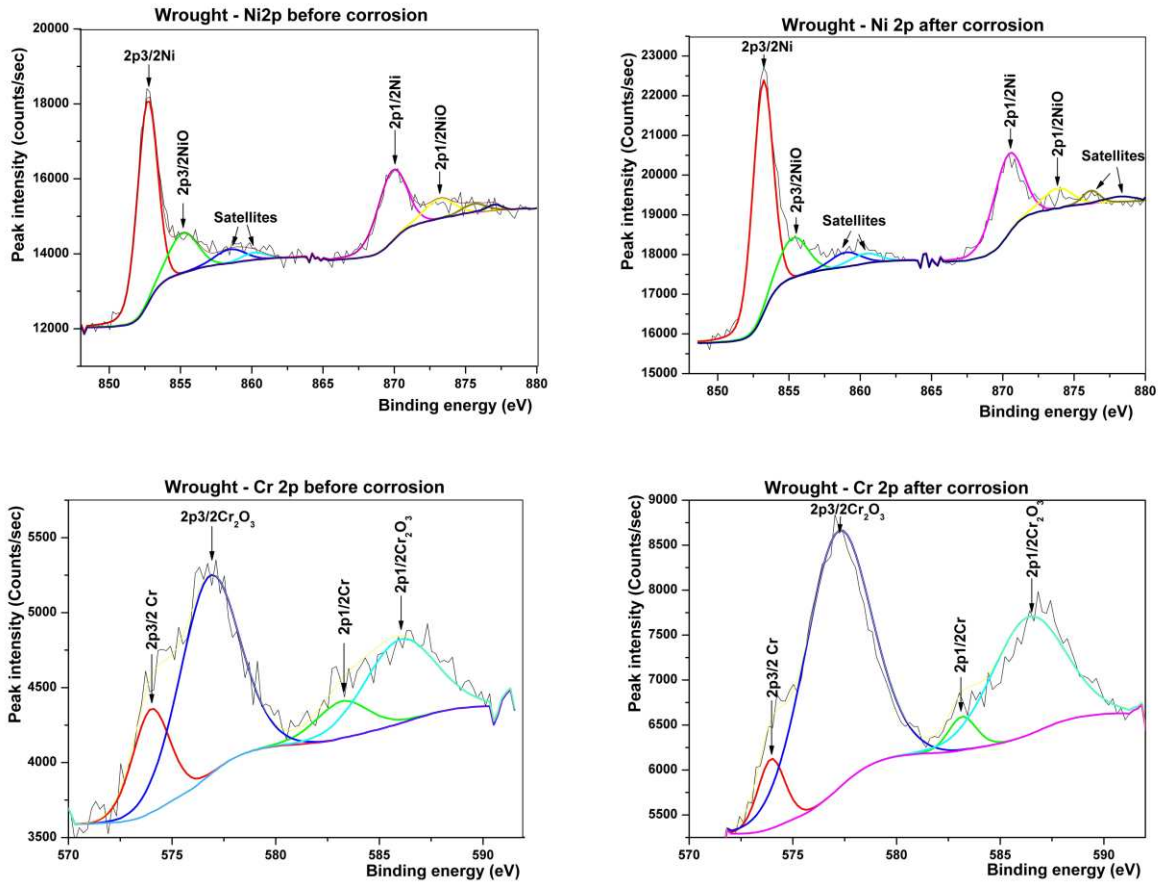

Figure **6** and Figure 8 are composed of a doublet peak corresponding to Cr^{2+}. The binding energy of 577eV identified this as Cr_2O_3. Peak area ratios indicated that the majority of the Cr present at the surface was oxidised, 88% of surface Cr in the coating was present as Cr_2O_3, compared to about 79% in wrought alloy. Fitting of the Nb3d single peak in the high resolution spectra in Figure 7 and **Error! Reference source not found.Figure 8** and at 205.42eV showed that it was formed from contributions from Nb^{2+} and Nb^{5+}, present in NbO and Nb_2O_5 respectively. No peak corresponding to the metallic state (Nb^0) was observed in either of the two samples. MoO_2 and MoO_3 were assigned in both samples along with metallic Mo. The proportion of Mo in the metallic state was 41% for the wrought material and 63% for the coating.

Overall, very similar results were seen for both samples.

3.3.2 Wrought alloy after polarisation corrosion test

The O 1s peak intensity and area were increased after polarisation, indicating more extensive oxidation. NiO was again the only nickel oxide identified. Area ratio results showed an increase in the proportion of Ni in the metallic state, from 61.1 to 73.6% after polarisation. The opposite effect was seen for Cr where the proportion of oxidised Cr increased from 79.6 to 83.3% after polarisation. The area ratio for Nb_2O_5 : NbO for $3d_{5/2}$ dramatically increased from 1.9 to 4.7 after polarisation, indicating oxidation of Nb^{2+} to Nb^{5+}, to form Nb_2O_5, a more stable oxide of Nb. There was no significant difference between the metallic peaks of molybdenum before and after corrosion (Figure 7).

3.3.3 Coating after polarisation corrosion test

As for the wrought material, the O1s peak intensity and area were increased after polarisation, indicating more extensive oxidation. There was little difference in the peak area ratios of Cr before and after polarisation, as shown in the high resolution spectra of $Cr2p_{3/2}$ and $Cr2p_{1/2}$ (Figure 8).

With regard to the Ni2p region, the distinct peak at a binding energy corresponding to 856.5eV was attributed to $Ni(OH)_2$ [7]. The XPS spectra again showed the presence of NiO.

There was a dramatic, ~50%, decrease in the proportion of metallic Mo and a corresponding increase in the total proportion of MoO_2 and MoO_3 (Figure 9).

As was the case before polarisation, no metallic Nb peak was observed. The $Nb3d_{5/2}$ peak area ratio of Nb_2O_5 : NbO increased from 2 to about 15 after polarisation.

4 Discussion

NiO, Cr_2O_3, MoO_2, MoO_3, NbO and Nb_2O_5 oxides were detected on samples of both wrought and coated Inconel 625 before polarisation. These are attributed to the air-formed film formed between sample polishing and XPS measurement and are consistent with previously reported XPS results from air-formed oxides on a nickel based alloy [14].

Previous XPS work on Inconel 625 has mentioned the Fe2p photoelectron peak at 707-720eV, however that peak is a minor feature in the spectra in this work, just visible as a shoulder on the Ni LMMb Auger peak in Figure 5a, and therefore has not been considered in our analysis.

Following polarisation of the wrought material the O1s peak increased indicating more extensive oxidation, however no additional species were detected. Some changes to the passive layer were noted. A larger proportion of the Cr2p peak was due to Cr_2O_3 whereas the metallic contribution to the Ni peak increased. There was also evidence of more extensive oxidation of Nb to Nb_2O_5, a compound that has previously been reported in XPS analysis of Inconel 625, albeit exposed to different conditions [15].

For the coating, polarisation in acid again increased the O1s peak, again indicating an increased extent of oxidation. This was consistent with the decreased proportion of the Mo peak attributed to metallic Mo and increased proportion of Nb_2O_5. In addition to this an extra peak, at 856.5eV was detected. This peak was attributed to $Ni(OH)_2$, a compound that was not detected in any of the other spectra recorded in this work. Its identification is supported not only by the binding energy value but also the relatively larger size of its satellite peak [16].

This work does not include any spatially resolved analysis of the oxide films formed. However, previous work [4, 6] has shown that partial oxidation during coating formation results in localised regions of the coating that are Ni-rich and Cr-depleted. Such areas have previously been identified as the cause of the lower corrosion resistance of

the sprayed coating compared to the wrought material [6]. Following the XPS results presented in this work it is suggested that during polarisation $Ni(OH)_2$ forms in these localised regions. $Ni(OH)_2$ is not as stable or as protective as the Cr, Mo and Nb oxides [13, 15]. Hence the presence of localised regions of $Ni(OH)_2$ limits the effectiveness of the passive film. This is consistent with the potentiodynamic results obtained in this work

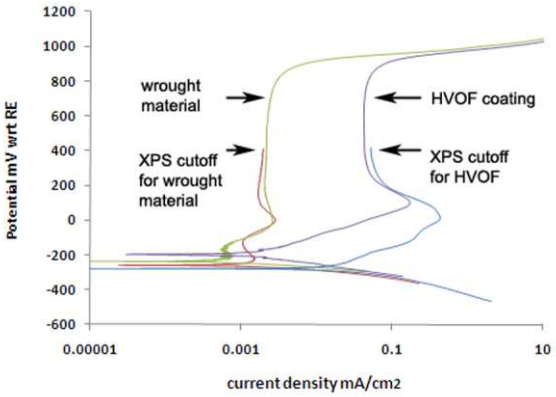

(Figure **1**), which indicate that the passive corrosion current density of the polarised coating is almost two orders of magnitude greater than that of the wrought material.

Summary and Conclusions

Previous work established that the performance gap in corrosion resistance between HVOF coatings and the corresponding bulk alloy was due to localised areas of different compositions formed by partial oxidation during coating formation [6]. The formation of $Ni(OH)_2$ on the polarised HVOF Inconel 625 coatings is attributed to these localised areas. Since $Ni(OH)_2$ does not form a protective, adherent, oxide the passive film is compromised and the corrosion resistance is inferior to that of the wrought material. The good corrosion resistance of wrought Inconel 625 is due to formation of Cr, Mo and Nb oxides.

- The air formed film on Inconel 625 consists of a mixture of NiO, Cr_2O_3, MoO_2, MoO_3, NbO and Nb_2O_5.

- The protective passive film formed on wrought Inconel 625 during polarisation also consists of NiO, Cr_2O_3, MoO_2, MoO_3, NbO and Nb_2O_5.

- The poorer corrosion resistance of the coating is attributed to the formation of loose, non-adherent non-protective $Ni(OH)_2$ during polarisation, in addition to the other oxides listed above.

- The formation of $Ni(OH)_2$ during polarisation of the coating is due to the presence of Ni-rich, Cr-depleted, regions formed as a result of partial oxidation during the coating process.

References

[1] V. Shankar, K. B. S. Rao and S. L. Mannan, J Nuc Mat 288 (2001) 222.
[2] D. Chidambaram, C. R. Clayton and M. R. Dorfman, Surf Coat Tech 176 (2004) 307.
[3] D. A. Walsh, L. E. Li, M. S. Bakare and K. T. Voisey, Electrochimica Acta 54 (2009) 4647.
[4] D. Zhang, S. J. Harris and D. G. McCartney, Mat Sci Eng A 344 (2003) 45.
[5] A. Neville, J. M. Perry, T. Hodgkiess and H. P. Chau, Proc Instn Mech Engrs 214 (2000) 41.
[6] N. Ahmed, M. S. Bakare, D. G. McCartney and K. T. Voisey, Surf Coat Tech 204 (2010) 2294.
[7] M. Sun, X. Wu, Z. Zhang and E.-H. Han, J Supercritical Fluids 47 (2008) 309.
[8] H. Sun, X. Wu and E.-H. Han, Cor Sci 51 (2009) 2565.
[9] A. C. Lloyd, J. J. Noël, S. McIntyre and D. W. Shoesmith, Electrochimica Acta 49 (2004) 3015.
[10] A. Neville and T. Hodgkiess, British Corrosion Journal 35 (2000) 183.
[11] P. Swift, Surface and Interface Analysis 4 (1982) 47.
[12] J. F. Moulder, W. F. Stickle, P. E. Sobol and K. D. Bomben, Handbook of X Ray Photoelectron Spectroscopy: A Reference Book of Standard Spectra for Identification and Interpretation of XPS Data (Eden Praire Minn., 1995).
[13] K. S. K. Danadurai, T. M. Sridhar, S. V. Narasimhan and S. Rajeswari, J Solid State Electrochemistry 4 (2000) 159.
[14] R. S. Dutta, Jagannath, G. K. Dey and P. K. De, Cor Sci 48 (2006) 2711.
[15] L. Tan, X. Ren, K. Sridharan and T. R. Allen, Cor Sci 50 (2008) 3056.
[16] H. W. Nesbitt, D. Legrand and G. M. Bancroft, Physics and Chemistry of Minerals 27 (2000) 357.

Tables

Elements	Ni	Cr	Mo	Nb	Fe	C	Mn	Si	Al	Ti
Wrought(wt %)	Bal.	20.9	9.13	3.41	3.27	0.01	0.07	0.07	0.1	0.21
Powder(wt %)	Bal.	21	9	3.46	0.12	0.03	0.1	0.1	-	-

Table 1: Percentage weight chemical composition of Inconel 625

Oxygen flow rate (l/min)	Fuel flow rate (l/min)	Nitrogen flow rate (l/min)	Nozzle length (mm)	Spray distance (mm)	Powder feed rate (g/min)	Number of passes
910	0.48	4.6	100	350	78.7	24

Table 2: HVOF coating spraying conditions

Samples	Wrought	Powder	As-sprayed coating
Oxide Content (weight%)	0.044±0.0004	0.086±0.0009	2.2±0.02
Porosity Content (%)	-	-	1.2±0.1

Table 3: Oxide and porosity content of samples

Figure captions

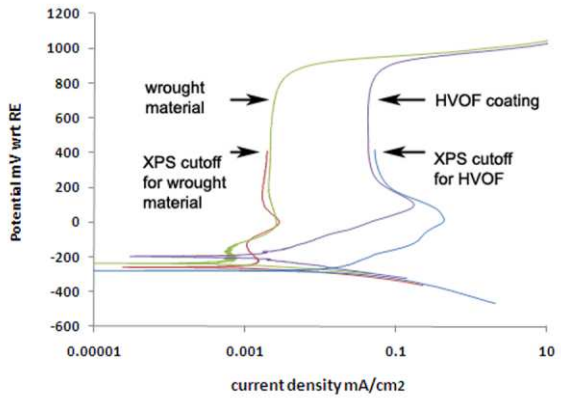

Figure 1: Potentiodynamic curves of samples showing the performance gap between wrought material and HVOF coating as well as the cut-off potentials of samples for XPS analysis.

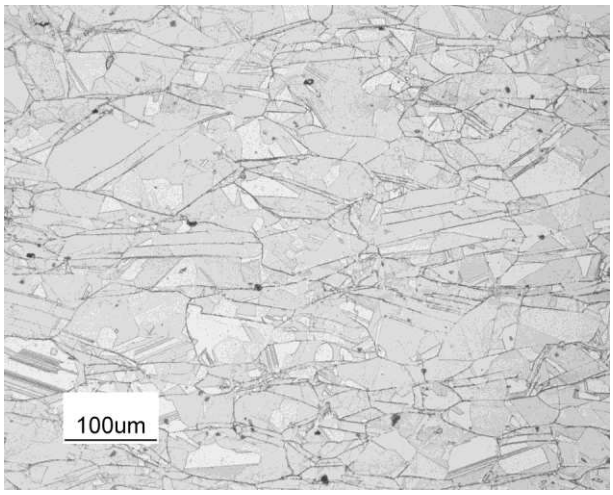

Figure 2: Optical micrograph of etched wrought Inconel 625.

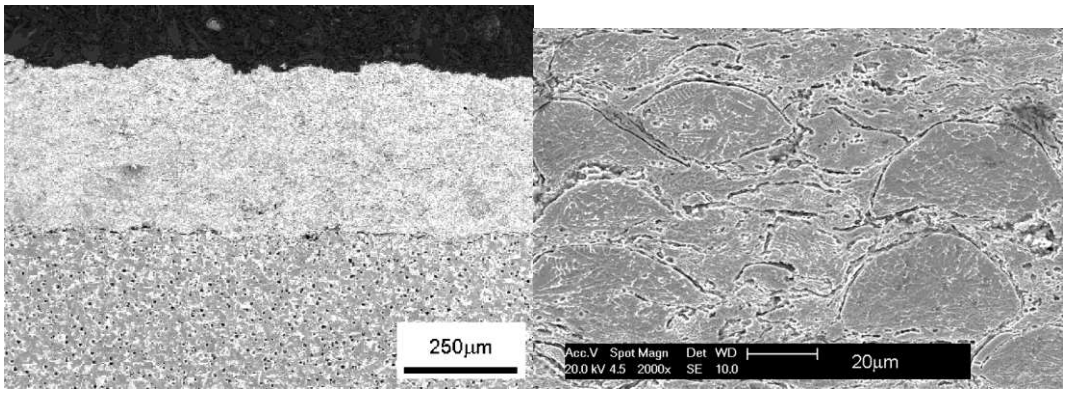

Figure 3: SEM image showing microstructure of the as-sprayed HVOF coating (a) low magnification cross-sectional image showing full coating thickness (b) higher magnification cross-sectional image showing splat structure.

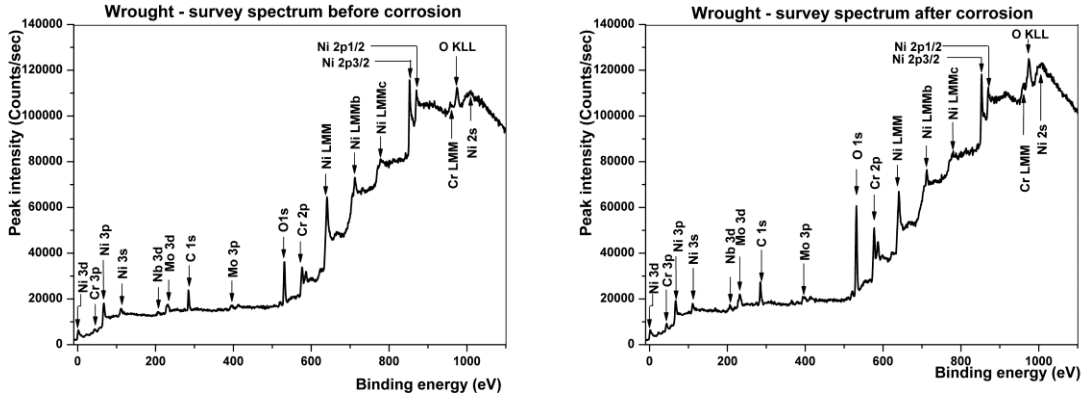

Figure 4: XPS survey spectra of wrought alloy before and after polarisation corrosion test.

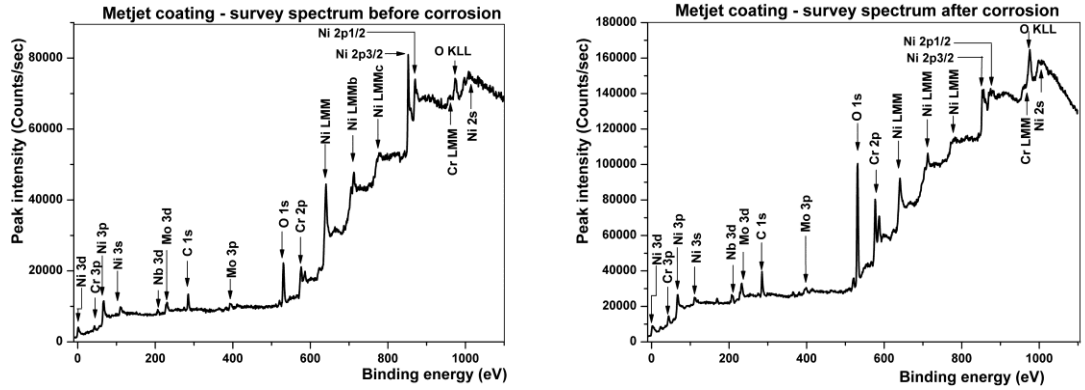

Figure 5: XPS survey spectra of HVOF coating before and after polarisation corrosion test.

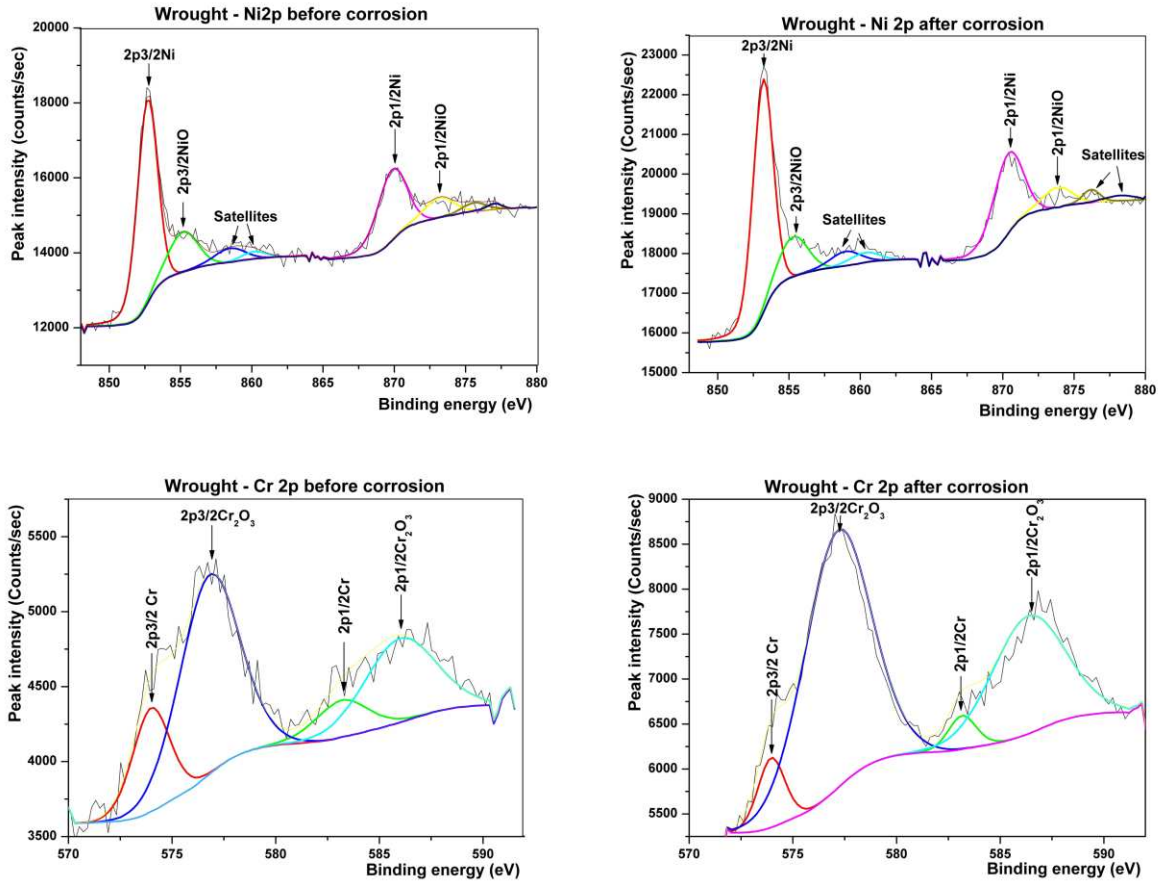

Figure 6: XPS high resolution spectra of Ni2p and Cr2p of wrought alloy before and after polarisation corrosion test.

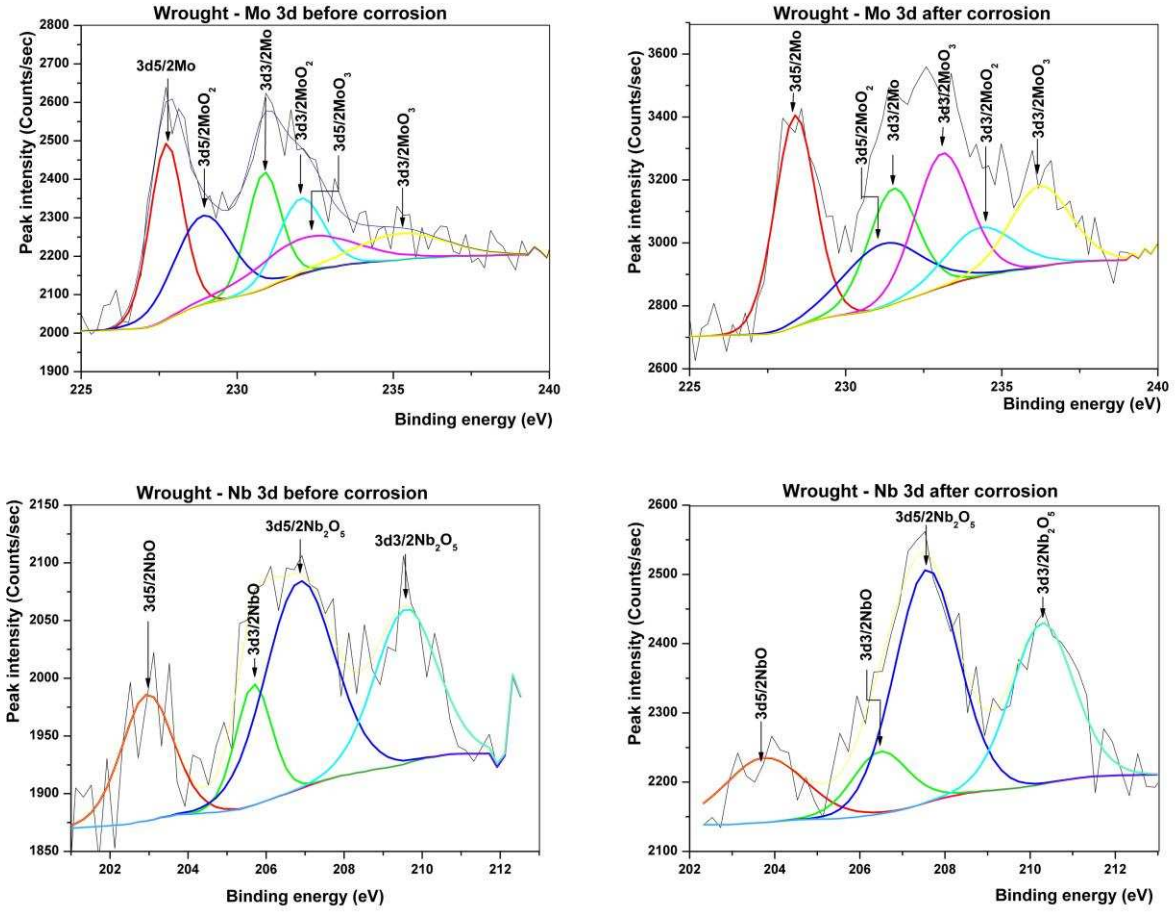

Figure 7: XPS high resolution spectra of Mo3d and Nb3d for wrought alloy before and after polarisation corrosion test.

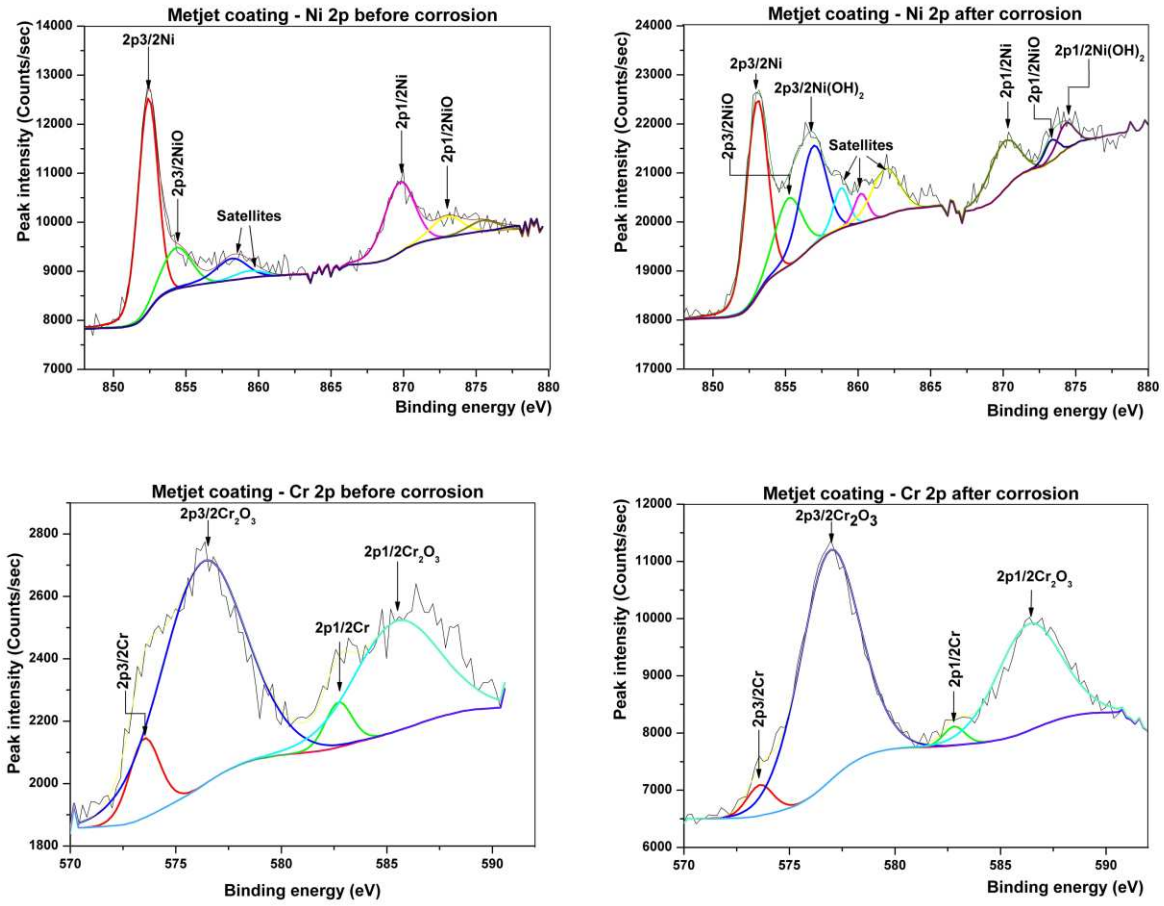

Figure 8: XPS high resolution spectra of Ni2p and Cr2p for HVOF coating before and after polarisation corrosion test.

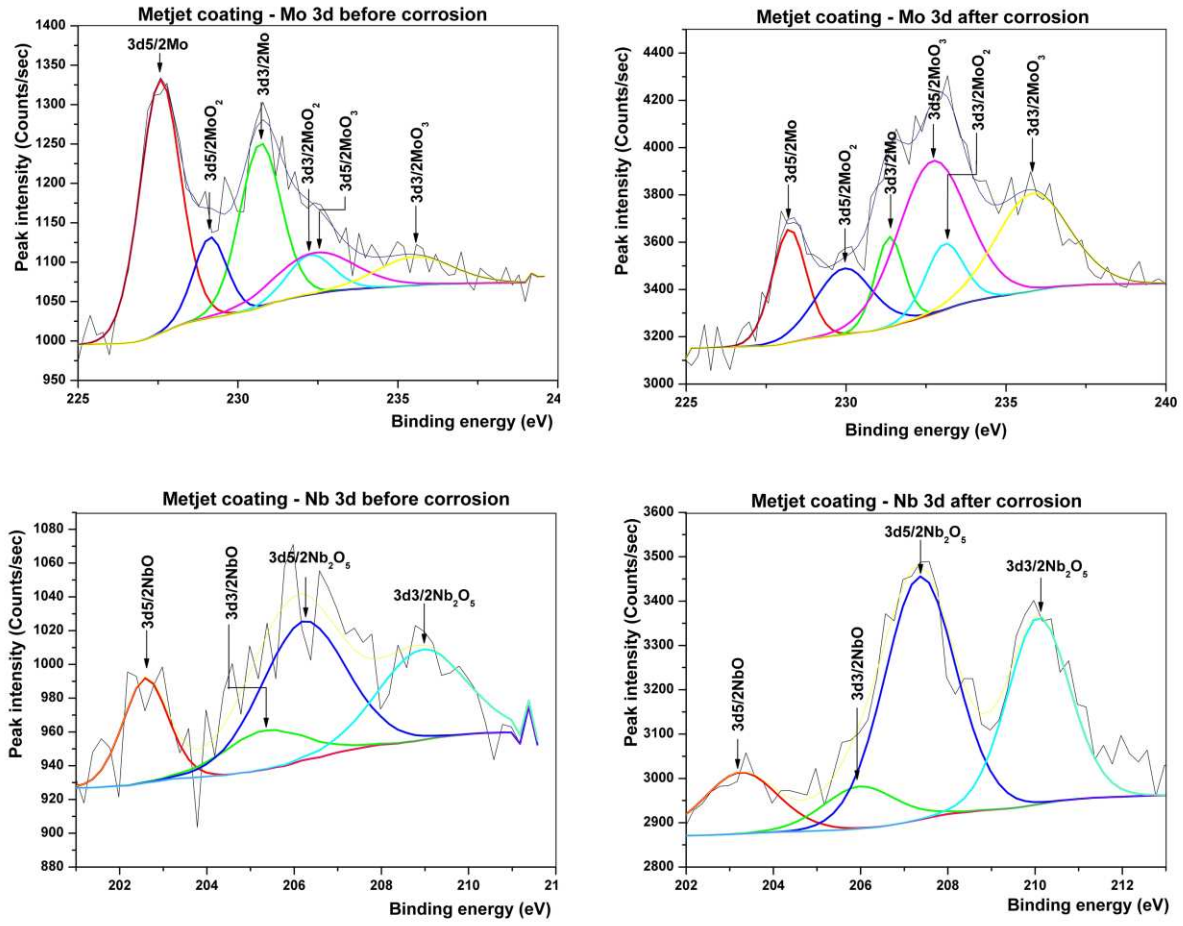

Figure 9: XPS high resolution spectra showing peaks of Mo3d for HVOF coating before and after polarisation corrosion test.

Appendices

	Wrought before Corrosion				Wrought after Corrosion			
Sample spectrum	**Binding energy (eV)**	**Proposed species**	**At. %**	**% area of peak**	**Binding energy (eV)**	**Proposed species**	**At. %**	**% area of Peak**
Survey spectrum	530.42	O 1s	50.1		531.38	O 1s	62.2	
	852.42	Ni 2p3/2	27.5		852.38	Ni 2p3/2	14.6	
	576.42	Cr 2p	16.0		577.38	Cr 2p	17.2	
	230.42	Mo 3d	4.6		231.38	Mo 3d	4.4	
	205.42	Nb 3d	1.8		206.38	Nb 3d	1.7	
High res spectrum Ni2p	852.68	2p 3/2Ni		46.3	853.17	2p 3/2Ni		47.2
	855.17	2p 3/2NiO		13.3	855.30	2p 3/2NiO		11.8
	858.48	2p 3/2Ni SAT		4.6	858.97	2p 3/2Ni SAT		4.3
	860.17	2p 3/2NiO SAT		2.0	860.30	2p 3/2NiO SAT		2.9
	869.82	2p 1/2Ni		23.6	870.34	2p 1/2Ni		24.1
	873.17	2p 1/2NiO		6.8	873.83	2p 1/2NiO		6.0
	875.62	2p 1/2Ni SAT		2.2	876.18	2p 1/2Ni SAT		2.2
	877.00	2p 1/2NiO SAT		1.0	877.33	2p 1/2NiO SAT		1.5
High res spectrum Cr2p	573.98	2p 3/2Cr		16.4	573.96	2p 3/2Cr		6.6
	583.18	2p 1/2Cr		8.3	583.16	2p 1/2Cr		3.3
	576.79	2p 3/2Cr_2O_3		50.1	577.14	2p 3/2Cr_2O_3		59.9
	586.99	2p 1/2Cr_2O_3		25.2	586.34	2p 1/2Cr_2O_3		30.2
High res spectrum Mo3d	227.73	3d 5/2Mo		24.3	228.38	3d 5/2Mo		24.7
	230.86	3d 3/2Mo		16.1	231.51	3d 3/2Mo		16.6
	228.90	3d 5/2MoO_2		21.3	231.17	3d 5/2MoO_2		14.4
	232.03	3d 3/2MoO_2		14.1	234.30	3d 3/2MoO_2		9.6
	232.10	3d 5/2MoO_3		14.6	233.09	3d 5/2MoO_3		20.8
	235.23	3d 3/2MoO_3		9.7	236.22	3d 3/2MoO_3		14.0
High res spectrum Nb3d	202.96	3d 5/2NbO		18.8	203.76	3d 5/2NbO		15.5
	205.68	3d 3/2NbO		12.6	206.48	3d 3/2NbO		10.4
	206.85	3d 5/2Nb_2O_5		41.1	207.56	3d 5/2Nb_2O_5		44.4
	209.57	3d 3/2Nb_2O_5		27.6	210.28	3d 3/2Nb_2O_5		29.8

Appendix A: Showing XPS detailed results for wrought alloy before and after polarisation corrosion test.

	As-sprayed HVOF coating before corrosion				As-sprayed HVOF coating after Corrosion			
Sample	**Binding**	**Proposed**	**At.**	**% area**	**Binding**	**Proposed**	**At.**	**% area**

spectrum	energy (eV)	species	% of peak	energy (eV)	species	% of peak
	530.38	O 1s	47.0	531.83	O 1s	64.9
Survey	852.38	Ni 2p3/2	30.2	852.83	Ni 2p3/2	12.2
spectrum	576.38	Cr 2p	16.8	576.83	Cr 2p	16.8
	230.38	Mo 3d	4.2	232.83	Mo 3d	3.8
	206.38	Nb 3d	1.8	206.83	Nb 3d	2.3
High res	852.38	2p 3/2Ni	44.2	853.03	2p 3/2Ni	31.6
spectrum	854.34	2p 3/2NiO	13.0	855.21	2p 3/2NiO	14.0
Ni2p	858.18	2p 3/2Ni SAT	6.8	856.91	2p 3/2$Ni(OH)_2$	19.9
	859.34	2p 3/2NiO SAT	2.2	858.83	2p 3/2Ni SAT	4.8
	869.70	2p 1/2Ni	22.5	860.21	2p 3/2NiO SAT	3.0
	873.00	2p 1/2NiO	6.6	861.91	2p 3/2Ni(OH)2 SAT	9.8
	875.50	2p 1/2Ni SAT	3.5	870.00	2p 1/2Ni	11.0
	878.00	2p 1/2NiO SAT	1.1	873.32	2p 1/2NiO	2.3
				874.32	2p 1/2$Ni(OH)_2$	3.6
High res	573.51	2p 3/2Cr	7.6	573.60	2p 3/2Cr	3.7
spectrum	582.71	2p 1/2Cr	3.8	582.80	2p 1/2Cr	1.9
Cr2p	576.26	2p 3/2Cr_2O_3	58.9	576.88	2p 3/2Cr_2O_3	62.8
	585.46	2p 1/2Cr_2O_3	29.7	586.33	2p 1/2Cr_2O_3	31.6
High res	227.57	3d 5/2Mo	38.0	228.22	3d 5/2Mo	12.7
spectrum	230.70	3d 3/2Mo	25.2	231.35	3d 3/2Mo	8.5
Mo3d	229.13	3d 5/2MoO_2	10.0	229.94	3d 5/2MoO_2	12.3
	232.26	3d 3/2MoO_2	6.6	232.07	3d 3/2MoO_2	8.3
	232.39	3d 5/2MoO_3	12.1	232.69	3d 5/2MoO_3	34.8
	235.52	3d 3/2MoO_3	8.0	235.82	3d 3/2MoO_3	23.4
High res	202.59	3d 5/2NbO	17.1	203.25	3d 5/2NbO	12.4
spectrum	205.31	3d 3/2NbO	11.5	205.97	3d 3/2NbO	8.3
Nb3d	206.21	3d 5/2Nb_2O_5	42.7	207.36	3d 5/2Nb_2O_5	47.4
	208.93	3d 3/2Nb_2O_5	28.7	210.08	3d 3/2Nb_2O_5	31.8

Appendix B: Showing XPS detailed results for HVOF coating before and after polarisation corrosion test.